PERGAMON

International Journal of Solids and Structures 36 (1999) 1231–1243

INTERNATIONAL JOURNAL OF SOLIDS and STRUCTURES

Scaling relationships in conical indentation of elastic-perfectly plastic solids

Yang-Tse Cheng[a,*], Che-Min Cheng (Zheng Zhemin)[b,1]

[a]*Physics and Physical Chemistry Department, General Motors Research and Development Center, Warren, Michigan 48090, U.S.A.*

[b]*Laboratory for Non-Linear Mechanics of Continuous Media, Institute of Mechanics, Chinese Academy of Sciences, Beijing 100080, P.R. China*

Received 2 July 1997; in revised form 3 November 1997

Abstract

Using dimensional analysis and finite element calculations we derive several scaling relationships for conical indentation into elastic-perfectly plastic solids. These scaling relationships provide new insights into the shape of indentation curves and form the basis for understanding indentation measurements, including nano- and micro-indentation techniques. They are also helpful as a guide to numerical and finite element calculations of conical indentation problems. Finally, the scaling relationships are used to reveal the general relationships between hardness, contact area, initial unloading slope, and mechanical properties of solids.

1. Introduction

Indentation experiments have been performed for nearly one hundred years for measuring the hardness of materials (Tabor, 1996). Recent years have seen increased interest in indentation because of the significant improvement in indentation equipment and the need for measuring the mechanical properties of materials on small scales. With the improvement in indentation instruments, it is now possible to monitor, with high precision and accuracy, both the load and displacement of an indenter during indentation experiments in the respective micro-Newtons and nano-meters ranges (Pethica et al., 1983; Stone et al., 1988; Bhushan et al., 1996). In addition to hardness, basic mechanical properties of materials, such as the Young's modulus, yield strength, and work hardening exponent, may be deduced from the indentation load vs displacement curves for loading and unloading. For example, the hardness and Young's modulus may be calculated

* Corresponding author. E-mail: yang_t._cheng@notes.gmr.com.

[1]E-mail: zhengzm@LNM.imech.ac.cn

0020–7683/99/$ - see front matter
PII: S0020–7683(97)00349–1

from the peak load and the initial slope of the unloading curves using the method of Oliver and Pharr (1992) or that of Doerner and Nix (1986). Finite element methods have also been used to extract the mechanical properties of materials by matching the simulated loading and unloading curves with the experimentally determined ones (Bhattacharya and Nix, 1988; Laursen and Simo, 1992; Bolshakov et al., 1996).

In spite of the significant progress made in recent years, the understanding of the general form of indentation loading and unloading curves is still lacking. In this paper, we derive, using dimensional analysis and finite element calculations, simple scaling relationships for indentation of elastic-perfectly plastic solids using a rigid conical indenter. These scaling relationships provide new insights into the shape of indentation curves and should, therefore, be useful to the interpretation of results obtained by instrumented indentation techniques, including nano- and micro-indentation measurements. They may also be helpful as a guide to numerical and finite element calculations of conical indentation problems. Finally, the scaling relationships can be used to reveal, as shown in the following, the general relationships between hardness, contact area, elastic, and plastic properties of solids.

2. Dimensional analysis

We consider a three-dimensional, rigid, conical indenter of a given half angle, θ, indenting normally into an elastic-perfectly plastic solid characterized by the Young's modulus (E), Poisson's ratio (v), and yield strength (Y). The friction coefficient at the contact surface between the indenter and the solid is assumed zero. Unlike the cases of indenting into elastic or rigid-plastic solids, this apparently simple problem involving elastic-perfectly plastic solids has in fact no analytical solution. However, dimensional analysis can be carried out to reveal the scaling relationships of conical indentation in elastic-perfectly plastic solids.

2.1. *Dimensional analysis of loading*

In general, the quantities of interest from the loading portion of indentation measurements include the force (F) and the contact depth under full load (h_c) (Fig. 1), from which the contact radius (a) and the hardness under full load (H) can be evaluated,

$$a = h_c \tan\theta, \tag{1}$$

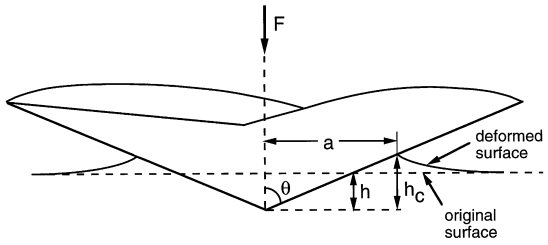

Fig. 1. Illustration of conical indentation.

$$H = \frac{F}{\pi a^2}. \tag{2}$$

The two dependent variables, F and h_c, must be functions, f_L and g, of all the independent governing parameters, namely, Young's modulus (E), Poisson's ratio (ν), yield strength (Y), indenter displacement (h), and the indenter half angle (θ):

$$F = f_L(E, Y, \nu, h, \theta), \tag{3}$$

$$h_c = g(E, Y, \nu, h, \theta). \tag{4}$$

Among the five governing parameters, E, Y, ν, h, and θ, two of them, namely E and h, have independent dimensions. The dimensions of Y, ν, θ, F, and h_c are then given by

$$\begin{aligned} [Y] &= [E], \\ [\nu] &= [E]^0[h]^0, \\ [\theta] &= [E]^0[h]^0, \\ [F] &= [E][h]^2, \\ [h_c] &= [h]. \end{aligned} \tag{5}$$

Applying the Π-theorem in dimensional analysis (Barenblatt, 1996), we obtain:

$$\Pi_\alpha = \Pi_\alpha(\Pi_1, \nu, \theta), \quad \text{or equivalently, } F = Eh^2\Pi_\alpha\left(\frac{Y}{E}, \nu, \theta\right), \tag{6}$$

$$\Pi_\beta = \Pi_\beta(\Pi_1, \nu, \theta), \quad \text{or equivalently, } h_c = h\Pi_\beta\left(\frac{Y}{E}, \nu, \theta\right), \tag{7}$$

where $\Pi_\alpha = F/Eh^2$, $\Pi_\beta = h_c/h$, $\Pi_1 = Y/E$, ν, and θ are all dimensionless.

Based on the above dimensional analysis, we can make several observations for a rigid conical indenter with a given half angle, θ, indenting into an elastic-perfectly plastic solid characterized by E, ν, and Y. First, the force on the indenter, F, is proportional to the square of the indenter displacement, h. Second, the contact depth, h_c, is proportional to the indenter displacement, h, or, the ratio, h_c/h, is independent of the indenter displacement. Furthermore, this ratio is only a function of Y/E and ν for a given θ.

2.2. *Dimensional analysis of unloading*

Since unloading takes place after loading during which the indenter reaches the maximum depth, h_m, the force, F, is now a function, f_U, of six independent governing parameters: Young's modulus (E), Poisson's ratio (ν), yield strength (Y), indenter displacement (h), the maximum depth (h_m), and the indenter half angle (θ)

$$F = f_U(E, Y, \nu, h, h_m, \theta). \tag{8}$$

Dimensional analysis yields

$$\Pi_\gamma = \Pi_\gamma(\Pi_1, \Pi_2, \nu, \theta), \quad \text{or equivalently, } F = Eh^2\Pi_\gamma\left(\frac{Y}{E}, \frac{h}{h_m}, \nu, \theta\right), \tag{9}$$

where $\Pi_\gamma = F/Eh^2$, $\Pi_1 = Y/E$, $\Pi_2 = h/h_m$, ν, and θ are all dimensionless.

In contrast to loading, eqn (9) shows that the force, F, is, in general, no longer simply proportional to the square of the indenter displacement, h. It also depends on the ratio, h/h_m, through the dimensionless function Π_γ.

We now consider the initial unloading slope dF/dh. Taking the derivative with respect to the indenter displacement and evaluating it at h_m, eqn (9) becomes:

$$\left.\frac{dF}{dh}\right|_{h=h_m} = Eh_m\left[\Pi'_\gamma\left(\frac{Y}{E}, 1, \nu, \theta\right) + 2\Pi_\gamma\left(\frac{Y}{E}, 1, \nu, \theta\right)\right]. \tag{10}$$

Consequently, the dimensionless quantity,

$$\frac{1}{Eh_m}\left.\frac{dF}{dh}\right|_{h=h_m} = \Pi'_\gamma\left(\frac{Y}{E}, 1, \nu, \theta\right) + 2\Pi_\gamma\left(\frac{Y}{E}, 1, \nu, \theta\right) \equiv \Pi_\delta\left(\frac{Y}{E}, \nu, \theta\right), \tag{11}$$

is independent of h/h_m and is a function, Π_δ, of only Y/E, ν, and θ. Equation (11) shows that the initial unloading slope is proportional to h_m in each indentation experiment for which E, ν, Y and θ are fixed.

3. Finite element analysis

Finite element calculations using ABAQUS (1996) have been carried out to illustrate the scaling relationships given by eqns (6), (7), and (11) and to evaluate the dimensionless functions $\Pi_\alpha(Y/E, \nu, \theta)$, $\Pi_\beta(Y/E, \nu, \theta)$, and $\Pi_\delta(Y/E, \nu, \theta)$. Following earlier work e.g., Bhattacharya and Nix (1988), the frequently used indenter half angle of 68° is chosen to illustrate the essential physics of conical indentation. To simplify notation, $\Pi_i(Y/E, \nu)$ $(i = \alpha, \beta, \delta)$ is used instead of $\Pi_i(Y/E, \nu, 68^\circ)$ $(i = \alpha, \beta, \delta)$. The dependence on indenter angle is implied.

Similar to previous finite element calculations, the large strain elasto-plastic feature of ABAQUS is used. In the finite element model shown in Fig. 2 the indenter and solid were modeled as bodies of revolution to take advantage of the axisymmetry of conical indentation. The indenter was modeled as a rigid body. The surface of the rigid indenter was defined using the ABAQUS feature of analytic rigid surface definition. The semi-infinite elastic-perfectly plastic solid was modeled using 3600 4-node bilinear axisymmetric quadrilateral elements. A fine mesh in the vicinity of the indenter and a gradually coarser mesh away from the indenter were used to ensure a high degree of numerical accuracy and a good representation of the semi-infinite solid. Indeed, the results were shown to be insensitive to the boundary conditions at the bottom and outer boundaries of the mesh. The loading and unloading curves were essentially the same (e.g., less than 0.4% and 1% changes in peak loads and initial unloading slopes, respectively) under three types of boundary conditions: (1) the bottom and outer surface nodes were fixed, (2) the outer surface nodes were traction-free with bottom surface nodes fixed, and (3) roller boundary conditions were applied to the bottom and outer surface nodes. Therefore, the mesh used provides a good approximation to

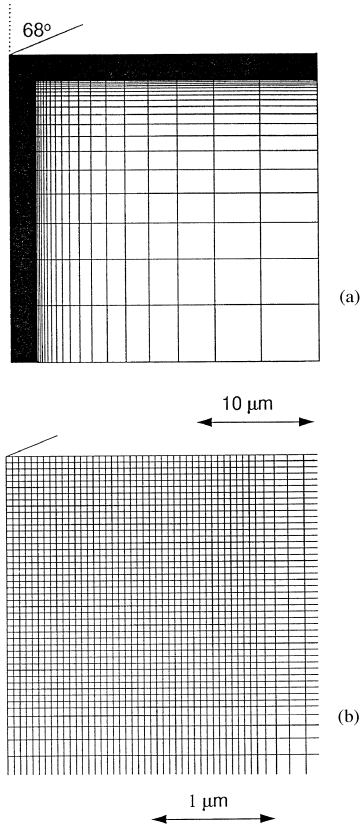

Fig. 2. Finite element mesh. (a) General view and (b) detailed view of the contact region.

a semi-infinite solid. The yield criterion was that of Mises. The loading and unloading curves were obtained directly from the ABAQUS output of the total reaction force in the normal direction on the rigid indenter as a function of indenter vertical displacement. The calculations were performed using ABAQUS version 5.5 and 5.6 on workstations.

Figure 3 shows two examples of the calculated loading and unloading curves for two sets of values of E, Y, v and several values of h_m. The loading curves were fitted with a power function: $F = ah^x$, where a and x are two fitting parameters. The exponent, x, obtained from all simulations, such as that shown in Fig. 3 is between 1.98 and 2.03. The simulation thus shows that the force, F, is proportional to the square of the displacement, h, for any set of values of E, v, and Y, as predicted from dimensional analysis, eqn (6).

Figure 4 displays the relationship between the calculated h_c and h for several sets of values of E, v, and Y. The predicted linear dependence, eqn (7), is evident. The contact depth, h_c, was obtained from the ABAQUS output of the surface profiles during the calculation of the loading curves. From Fig. 4 it is apparent that the ratio h_c/h can be either greater or smaller than one, corresponding to the "piling-up" and "sinking-in" of the displaced surface profiles, respectively.

Figure 3 also shows examples of unloading curves calculated for various h_m. The unloading

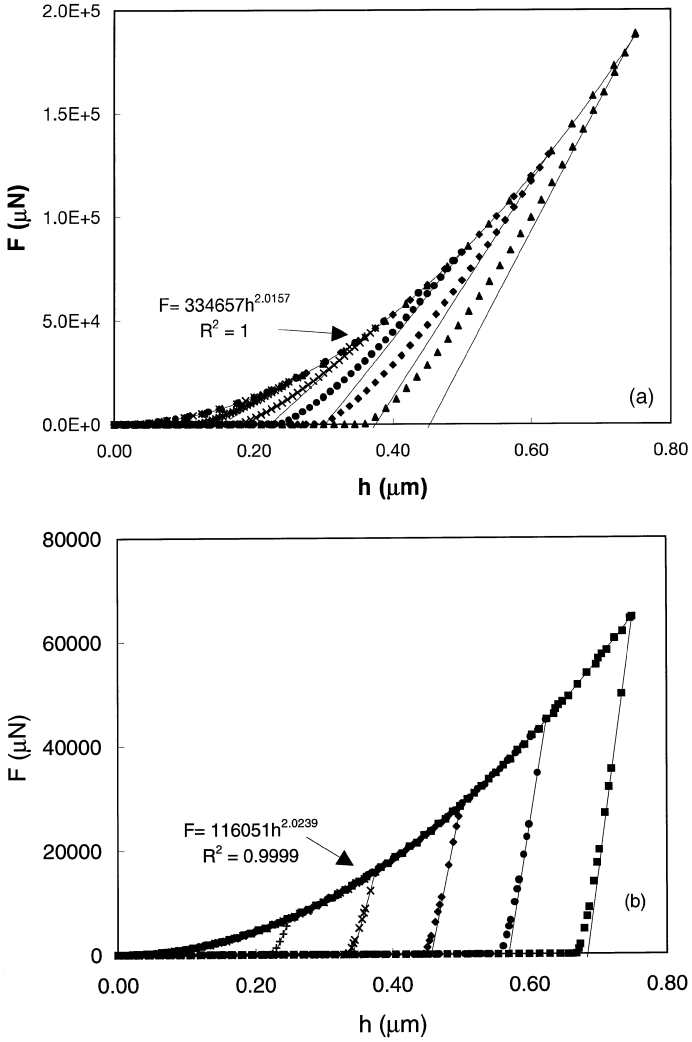

Fig. 3. Indentation curves obtained from finite element analysis. (a) For $E = 200$ GPa, $v = 0.3$, and $Y = 20$ GPa and (b) For $E = 200$ GPa, $v = 0.3$ and $Y = 2.0$ GPa. The initial unloading slopes are also shown.

slope was obtained from a linear fit to the first two or three points on the unloading curves. (Care was taken so that the two or three points are sufficiently close together to represent initial unloading.) The initial unloading slopes are plotted against the maximum depth h_m in Fig. 5 for several sets of values of E, v, and Y. A linear relationship between the initial unloading slope and the maximum depth for each set of values of E, v and Y is evident, confirming the predictions by eqn (11).

To evaluate the dimensionless functions, $\Pi_i(Y/E, v)$ $(i = \alpha, \beta, \delta)$, simulations were performed for a large number of Y and a few selected values of E and v. Figures 6, 7, and 8 display the respective F/Eh^2, h_c/h, and

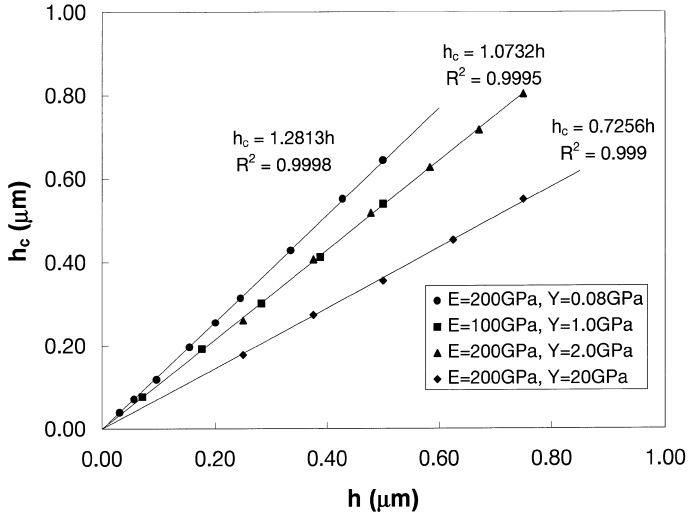

Fig. 4. Relationships between contact depth, h_c, and indenter displacement, h, obtained from finite element calculations for several cases of E and Y with $v = 0.3$.

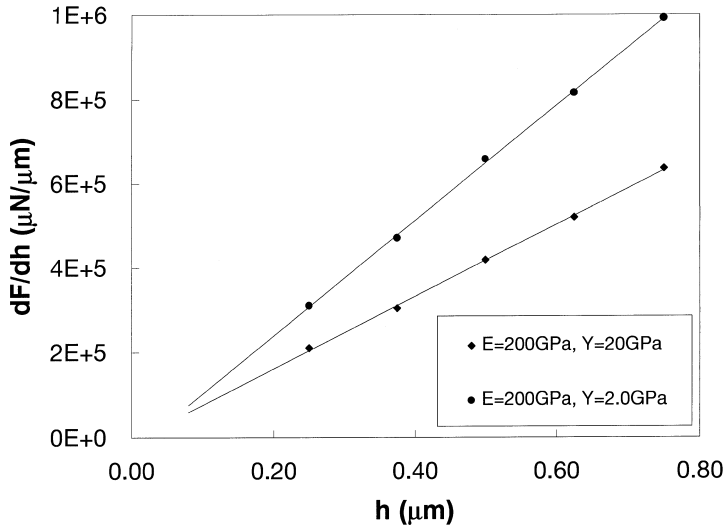

Fig. 5. Relationships between initial unloading slope, dF/dh, the indenter displacement, h, obtained from finite element calculations for two cases of E and Y with $v = 0.3$.

$$\frac{1}{Eh_m}\frac{dF}{dh}\bigg|_{h=h_m} \text{ vs } Y/E.$$

It is evident from Fig. 6 that, for a given value of v, the quantity $(F/Eh^2, Y/E)$ lies on a single curve. Thus, F/Eh^2 is a function of Y/E and v, as predicted by dimensional analysis, i.e.,

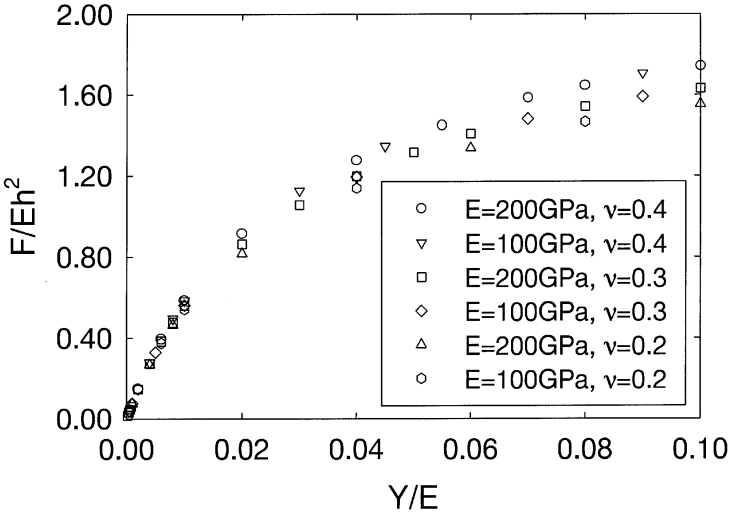

Fig. 6. Scaling relationships between F/Eh^2 and Y/E.

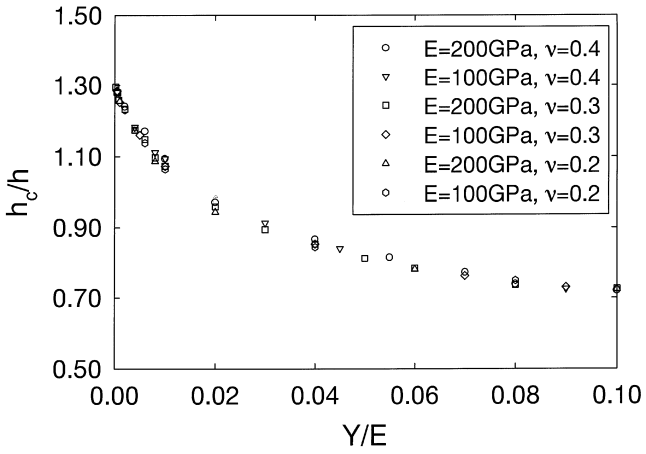

Fig. 7. Scaling relationships between h_c/h and Y/E.

$F/Eh^2 = \Pi_\alpha(Y/E, v)$. Similarly, Fig. 7 suggests that h_c/h is insensitive to v and is a function of only Y/E, i.e., $h_c/h = \Pi_\beta(Y/E, v) \approx \Pi_\beta(Y/E)$. Finally, Fig. 8 shows that

$$\frac{1}{Eh_m}\frac{dF}{dh}\bigg|_{h=h_m} = \Pi_\delta(Y/E, v).$$

Thus, simple scaling relationships, such as that given by eqns (6), (7), and (11) exist for a rigid conical indenter indenting into elastic-perfectly plastic solids. Although the numerical values of the dimensionless functions, $\Pi_i(Y/E, v, \theta)$ $(i = \alpha, \beta, \delta)$, have been calculated for a particular indenter

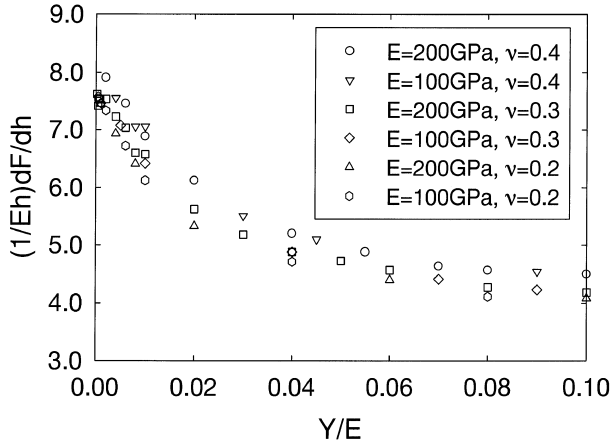

Fig. 8. Scaling relationships between $(1/Eh)\,\mathrm{d}F/\mathrm{d}h$ and Y/E.

angle (e.g., $\theta = 68^\circ$), similar finite element calculations can obviously be performed for other angles of interest.

4. Discussion

As an application of the scaling relationships, we consider the relationship between hardness and elastic and plastic properties of solids. Using eqns (1), (2), (6) and (7) the ratio of hardness of yield strength is given by

$$\frac{H}{Y} = \frac{\cot^2(\theta)}{\pi}\left[\frac{\Pi_\alpha\left(\frac{Y}{E}, \nu, \theta\right)}{\frac{Y}{E}\Pi_\beta^2\left(\frac{Y}{E}, \nu, \theta\right)}\right]. \tag{12}$$

Clearly, the hardness is independent of the depth of indentation, h. The ratio H/Y is, in principle, a function of Y/E and ν, as well as indenter geometry (θ). Taking $\theta = 68^\circ$ for example, the dependence of H/Y on Y/E and ν is illustrated in Fig. 9. It is apparent that, over the practically relevant range of Y/E, the ratio H/Y is not a constant. The hardness, H, depends on Y, E, and, to a lesser extent, ν. However for most metals for which $0 < Y/E < 0.01$, the ratio H/Y is between 2.5 and 2.6. This ratio H/Y is never 3, which was observed in indentation into metals using spherical indenters (Tabor, 1996; Johnson, 1985). Furthermore, the ratio H/Y decreases with increasing Y/E.

Also plotted in Fig. 9 is the prediction of H/Y given by Johnson's spherical cavity model for conical indentation into elastic-perfectly plastic solids (Johnson, 1970, 1985):

$$\frac{H}{Y} = \frac{2}{3}\left\{1 + \ln\left[\frac{E}{6Y(1-\nu)}\cot\theta + \frac{2}{3}\frac{1-2\nu}{1-\nu}\right]\right\}. \tag{13}$$

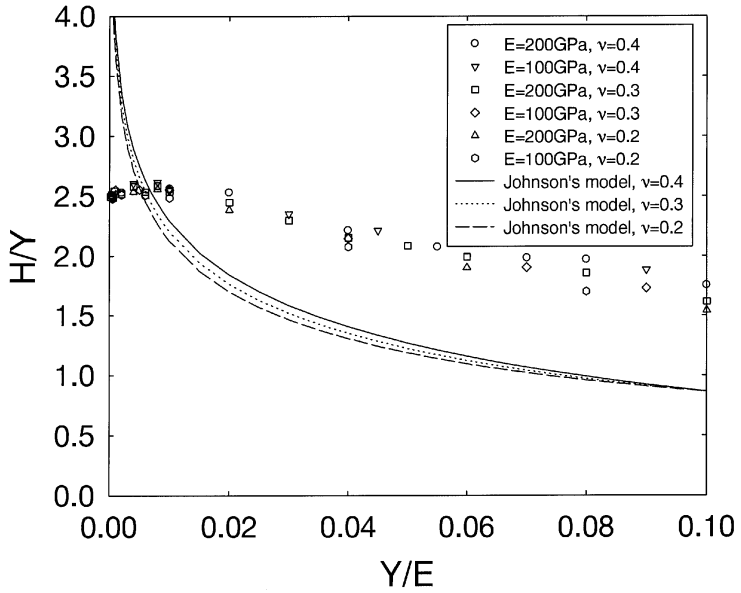

Fig. 9. Relationships between H/Y and Y/E determined by finite element calculations and that by Johnson's spherical cavity model.

In deriving eqn (13) Johnson idealized the surface profiles by neglecting piling-up and sinking-in effects. It is thus expected that Johnson's model could overestimate H for small Y/E where "piling-up" occurs and underestimate H for large Y/E where "sinking-in" occurs. Finite element calculations, on the other hand, take into account the effects of piling-up and sinking-in on hardness.

As a second application of the scaling relationships, we consider the relationship between the initial unloading slope, the contact radius, and Young's modulus of materials. Using eqns (1), (7), and (11) we obtain

$$\frac{1-v^2}{Ea}\left.\frac{\mathrm{d}F}{\mathrm{d}h}\right|_{h=h_{\mathrm{m}}} = \frac{1-v^2}{\tan\theta}\left[\frac{\Pi_\delta\left(\dfrac{Y}{E}, v, \theta\right)}{\Pi_\beta\left(\dfrac{Y}{E}, v, \theta\right)}\right]. \tag{14}$$

We evaluate eqn (14) for $\theta = 68^\circ$ and plot it against Y/E in Fig. 10. It is apparent from Fig. 10 that this quantity is roughly independent of Y/E and v and is given by

$$\left.\frac{1-v^2}{Ea}\frac{\mathrm{d}F}{\mathrm{d}h}\right|_{h=h_{\mathrm{m}}} \approx 2.16 \pm 0.08. \tag{15}$$

In fact, Fig. 10 and eqn (15) illustrate a special case of a general relationship between the initial unloading slope, the contact radius, Young's modulus, and Poisson's ratio:

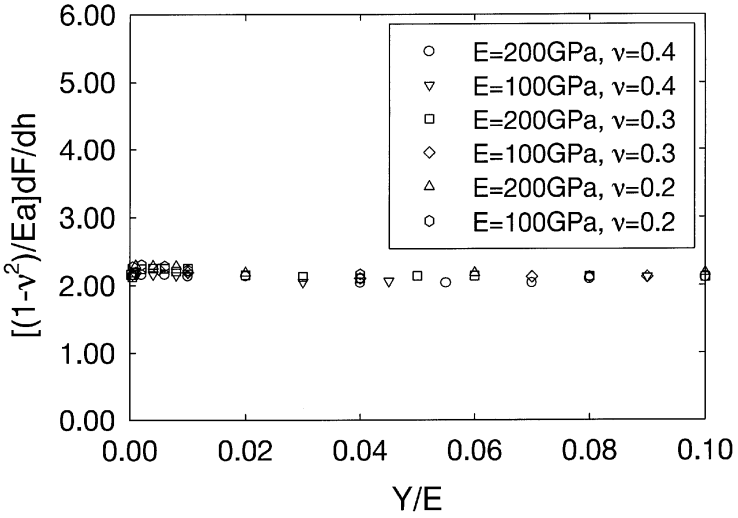

Fig. 10. A relationship between $\frac{1-v^2}{Ea}\frac{\mathrm{d}F}{\mathrm{d}h}\Big|_{h=h_{\mathrm{m}}}$ and Y/E.

$$\frac{1-v^2}{Ea}\frac{\mathrm{d}F}{\mathrm{d}h}\Big|_{h=h_{\mathrm{m}}} = 2. \tag{16}$$

Although eqn (16) was initially derived for indentation into elastic solids (Sneddon, 1963; Pharr et al., 1992), we have recently generalized it to the initial unloading in elastic–plastic solids using indenters with axisymmetric smooth profiles (Cheng and Cheng, 1997). Furthermore, we have shown that eqn (16) should hold true even for materials with work hardening and initial stress. While eqn (16) was derived using linearized boundary conditions, finite element calculations take into account nonlinear effects, including large strain and moving contact boundaries. Therefore, the small difference in numerical values between that given by eqns (15) and (16) is not unexpected. In practice, either equation may be used to estimate the elastic constant, $(1-v^2)/E$, from the initial slope of unloading curves, provided that the contact radius is known.

5. Summary

Using dimensional analysis and finite element calculations we have derived several scaling relationships for conical indentation into elastic–perfectly plastic solids. We have shown that, for loading, the force on the indenter is proportional to the square of the indenter displacement. The contact depth is proportional to the indenter displacement. For unloading, the initial unloading slope is proportional to the depth of indentation.

Using these scaling relationships we have determined relationships between hardness, contact area, initial unloading slope, and mechanical properties of solids. Specifically, the ratio of hardness to yield strength (H/Y) is shown to be a function of the ratio of yield strength to Young's modulus (Y/E) and Poisson's ratio (v). The functional dependence is significantly different from that

predicted by Johnson's spherical cavity model for conical indentation. This difference is most likely caused by the fact that the spherical cavity model does not take into account the sinking-in or piling-up of surfaces around indenters. We have also shown that, although the contact radius, a, and the initial unloading slope, $\mathrm{d}F/\mathrm{d}h$, at a given indenter displacement are both functions of Y/E and v, the ratio,

$$\frac{1-v^2}{Ea}\frac{\mathrm{d}F}{\mathrm{d}h},$$

is roughly a constant. Thus, the elastic constant, $E/(1-v^2)$, can indeed be evaluated from the initial unloading slope, provided that the contact radius is known.

Although the scaling relationships have been derived for conical indentation, the same approach can be applied to indentation using pyramidal indenters, since pyramidal indenters are also geometrically self-similar. Consequently, the scaling approach should form the basis for understanding indentation measurements using both conical and pyramidal indenters. They could also be helpful as a guide to numerical and finite element calculations of conical and pyramidal indentation problems.

These scaling relationships may also be used to detect the experimentally encountered "indentation size effect". It has been frequently reported that the apparent hardness increases or, sometimes, decreases as the size of the indent decreases in conical and pyramidal indentation experiments. A number of suggestions have been put forward to explain this indentation size effect, including the formation of microcracks under the indenter (Quinn and Quinn, 1997), the influence of a hard surface layer, and a dependence of flow strength on the gradients of plastic strain (Poole et al., 1996). In some cases, the indentation size effect has been shown to be an experimental artifact, caused by the incorrect determination of the contact area (Iost and Bigot, 1996). The scaling relationships derived in this study are necessary consequences of conical or pyramidal indentation in a homogeneous solid without an intrinsic length scale. Accordingly, deviations from these scaling relationships suggest the existence of such intrinsic length scale. The scaling relationships can, therefore, be used to detect the "indentation size effect" caused by some intrinsic length scale. However, a general theory for indentation size effects is clearly beyond the scope of conical indentation in elastic-perfectly plastic solids and requires future studies.

Acknowledgements

We would like to thank W. J. Meng, S. J. Harris, G. L. Eesley, J. R. Smith, L. C. Lev, W. J. Baxter, W. H. Yang, D. D. Snyder and K. C. Taylor for helpful discussions. We would also like to thank R. J. Blint, M. S. Meyer, K. Ueno, P. C. Wang, J. Brown (EDS), P. Lalor (HKS) and L. Hill (HKS) for helping with the use of ABAQUS and for maintaining the workstations.

References

ABAQUS (1996) Version 5.6. Hibbitt, Karlsson & Sorensen, Inc., Pawtucket, RI 02860, U.S.A.

Barenblatt, G. I. (1996) *Scaling, Self-Similarity, and Intermediate Asymptotics*. Cambridge University Press, Cambridge, U.K.

Bhattacharya, A. K. and Nix, W. D. (1988) *International Journal of Solids and Structures* **24,** 881.
Bhushan, B., Kulkarni, A., Bonin, W. and Wyrobek, J. (1996) *Phil. Mag*. **A74,** 1117.
Bolshakov, A., Oliver, W. C. and Pharr, G. M. (1996) *J. Mat. Res*. **11,** 760.
Cheng, C.-M. and Cheng, Y.-T. (1997). *Applied Physics Letters* **71,** 2623.
Doerner, M. F. and Nix, W. D. (1986) *J. Mat. Res*. **1,** 601.
Johnson, K. L. (1970) *Journal of Mechanics and Physics of Solids* **18,** 115.
Johnson, K. L. (1985) *Contact Mechanics*. Cambridge University, Cambridge, U.K.
Iost, A. and Bigot, R. (1996) *J. Mat. Sci*. **31,** 3573.
Laursen, T. A. and Simo, J. C. (1992) *J. Mat. Res*. **7,** 618.
Oliver, W. C. and Pharr, G. M. (1992) *J. Mat. Res*. **7,** 1564.
Pethica, J. B., Hutchings, R. and Oliver, W. C. (1983) *Phil. Mag*. **A48,** 593.
Pharr, G. M., Oliver, W. C. and Brotzen, F. R. (1992) *J. Mat. Res*. **7,** 613.
Poole, W. J., Ashby, M. F. and Fleck, N. A. (1996) *Scripta Materialia* **34,** 559.
Quinn, J. B. and Quinn, G. D. (1997) *J. Mat. Sci*. **32,** 4331.
Sneddon, I. N. (1963) *Int. J. Eng. Sci*. **3,** 47.
Stone, D., LaFontaine, W. R., Alexopoulos, P., Wu, T. W. and Li, C.-Y. (1988) *J. Mat. Res*. **3,** 141.
Tabor, D. (1996) *Phil. Mag*. **A74,** 1207.